

Fast and optimal centroiding of faint stars

Mohammadjavad Vakili¹, David W. Hogg^{1,2,3}

`mjvakili@nyu.edu`

ABSTRACT

One of the most demanding tasks in astronomical image processing—in terms of precision—is the centroiding of stars. Upcoming large surveys are going to take images of billions of point sources, including many faint stars, with short exposure times. Real-time estimation of the centroids of stars is crucial for real-time PSF estimation, and maximal precision is required for measurements of proper motion. In this work, we aim to compare the performance of various centroiding methods, when they are applied to relatively low signal-to-noise ratio unsaturated stars. In order to investigate how information-preserving these techniques are, we compare the root-mean-squared-error with the fundamental Cramér-Rao lower bound assuming zero-mean constant Gaussian noise. We discuss two general circumstances in centroiding of faint stars: (i) when we have a good estimate of the PSF, (ii) when we do not know the PSF. In the case that we know the PSF, we show that a fast polynomial centroiding after smoothing the image by the PSF can be as accurate as full PSF profile fitting. In the case that we do not know the PSF, we demonstrate that although polynomial centroiding is not as accurate as PSF profile fitting, it comes close to saturating the Cramér-Rao lower bound in a wide range of conditions. We also show that the moment-based methods of center-of-light never comes close to saturating the bound, and thus it does not deliver reliable estimates of centroids.

1. Introduction

Accuarate estimates of the centers of point sources, which are convolved with telescope point spread function (and atmospheric PSF in case of ground based telescopes), and also

¹Center for Cosmology and Particle Physics, Department of Physcs, New York University, 4 Washington Pl., room 424, New York, NY, 10003, USA

²Max-Planck-Institut für Astronomie, Königstuhl 17, D-69117 Heidelberg, Germany

³Center for Data Science, New York University, 726 Broadway, 7th Floor, New York, NY 10003, USA

the pixel response function, are crucial to further steps of astronomical image processing. For instance, proper measurement of the shapes of galaxies requires interpolation of the PSF estimates from the positions of stars across the image to the positions of galaxies. At the position of each star, the PSF is wrongly estimated by sub-pixel shifting of the star so that it is centered on its centroid. If the sub-pixel shifts are wrong, then the PSF estimates will be biased. Moreover, measurements of the parallaxes and the proper motions of stars depends on how well we can measure their centroids.

Ideally, we want a centroiding procedure that provides measurements as precise as possible, without putting a huge computational burden on the photometric pipeline. Reducing the computational cost becomes even more important in large surveys, where we want to estimate the centroids of thousands of point sources detected on the telescope’s focal plane, for various real-time applications.

In this paper, we study the optimality of various techniques for centroiding faint, unsaturated stars. That is, we apply a number of centroiding methods to a large number of simulated faint stars, assuming uncorrelated Gaussian noise, with different signal-to-noise ratio and size realizations. Error from star centroiding methods, will always have a theoretically-set lower bound, known as the Cramér-Rao lower bound (hereafter denoted by CRLB) which has an inverse relation with the signal-to-noise-ratio of stars.

Reaching the optimal measurement of the centroids of stars however, is limited by the lack of knowledge about the exact shape of the PSF, and also presence of noise; both sky noise and CCD readout noise. Thus, of particular interest is devising a fast method that returns optimal estimates of centroids in a realistic range of signal-to-noise ratios.

To date, a number of softwares packages have been designed for the purpose of extracting astronomical sources and making catalogs. One of these softwares is SExtractor ([Bertin & Arnouts 1996](#)), whose centroiding method involves first finding the zeroth moment of the object as a first-order estimate, and then iteratively correcting the centroid by computing the zeroth order moment of the object weighted by a Gaussian window function, until the correction falls below a particular threshold value. The width of the Gaussian window function is set by the object’s half-light radius. Other examples are DAOPHOT ([Stetson 1987](#)), and DOPHOT ([Schechter et al. 1993](#)) which both assume analytic models for the stellar PSF profiles with centroid coordinates being free parameters of these models. DAOPHOT (DoPHOT) finds the centroids by fitting a Gaussian (a truncated power series for a Gaussian) PSF to the light profile of stars.

Given an analytic expression for the PSF model, we derive an expression for the fundamental lower bound on the centroiding error as a function of the parameters of the PSF

model (*e.g.*PSF size), and signal-to-noise-ratio of stars. We create two sets of simulations for which we know the CRLB, one with variable signal-to-noise ratio and constant FWHM, and one with variable FWHM and constant signal-to-noise ratio. After applying different centroiding methods to the simulations, we investigate how close these methods can get to saturating the CRLB for various ranges of background noise level and PSF FWHM.

In this work, we focus on four centroiding methods. The first method involves fitting a PSF profile, assuming that we have a good PSF estimate, to the star. The second method estimates the centroid of a star by fitting a 2d second-order polynomial to the 3×3 patch around the brightest pixel of the image after convolution with the PSF. The third method centroids stars by smoothing the image of stars by a Gaussian kernel of a fixed size, and then applying the same 3×3 polynomial trick to the smooth image. This method is fast and does not require any knowledge of the PSF. The last method we consider, is a center of light centroiding (measurement of a first moment), applied to the 7×7 patch around the brightest pixel of the image.

This paper is structured as follows. In Section 2, we discuss the Cramér-Rao lower bound, and we derive an analytic expression for the lower bound on centroiding error of the simulated data, and also PSF profile fitting. In Section 3 we give a brief overview of approximate centroiding methods used in our investigation. In Section 4 we discuss the Cramér-Rao lower bound saturation tests and their corresponding simulated data. In Section 5, we compare the performances of the methods discussed in 3, with the CRLB derived in 4. Finally, we discuss and conclude in Section 6.

2. Cramér-Rao lower bound

Cramér-Rao lower bound sets a limit, in some sense, on how well a measurement can be made in noisy data. The bound can only be computed in the context of a generative model, or a probabilistic forward model of the data. That is, we can only compute the CRLB in the context of assumptions about the properties of the data. However, it makes sense for us to use centroiding methods that saturate the CRLB under some reasonable assumptions, even if we find that those assumptions are slightly wrong in detail in real situations.

In order to test the accuracy of various centroiding methods, we need to compare their performances against each other at saturating the Cramér-Rao lower bound on centroiding error. The closer an estimator is to saturating the CRLB, the more information about the quantity that we need to estimate is preserved. The closer the root-mean-squared-error of a given estimator is to the bound, the more optimal the estimator is.

The Cramér-Rao inequality (Cramér 1946) sets a lower bound on the root-mean-squared error of unbiased estimators. The CRLB is given by square-root of the inverse of the Fisher information matrix \mathcal{F} . Thus, in order to find the CRLB, it is sufficient to compute the Fisher matrix.

Let us assume that there are M observables $\mathbf{f} = (f_1, \dots, f_M)$, each related to B model parameters $\boldsymbol{\theta} = (\theta_1, \dots, \theta_B)$

$$f_m = f_m(\theta_1, \dots, \theta_B). \quad (1)$$

Assuming uncorrelated Gaussian error with variance σ_m^2 for each observable f_m , elements of the $B \times B$ Fisher matrix \mathcal{F}_{ij} are given by

$$\mathcal{F}_{ij} = \sum_{m=1}^M \frac{1}{\sigma_m^2} \frac{\partial f_m}{\partial \theta_i} \frac{\partial f_m}{\partial \theta_j} \quad (2)$$

Let us assume that, for each parameter θ_i , there exists a set of unbiased estimators $\{\hat{\theta}_i\}$. The Cramér-Rao inequality states that the root-mean-squared error of this set is greater than or equal to the i -th diagonal element of the inverse of the Fisher information matrix:

$$\text{RMSE}[\{\hat{\theta}_i\}] \geq \sqrt{[\mathcal{F}^{-1}]_{ii}}, \quad (3)$$

where the left hand side of the inequality is called the Cramér-Rao bound on the root-mean-squared error of estimating the parameter θ_i . Note that the bound is computed assuming that the model (1) generating the data is known, and that uncertainties are given by additive uncorrelated Gaussian noise.

Based on inequality (3), Cramér (1946) defines efficiency of unbiased estimators as the ratio of the CRLB and the root-mean-squared-error such that the maximum efficiency achievable by an estimator is unity. The closer the root-mean-squared to the CRLB, the more information about the parameter of interest is preserved, and thus the more efficient the estimator is.

Let us consider the case of maximum likelihood estimate $\boldsymbol{\theta}_{\text{ML}}$

$$\boldsymbol{\theta}_{\text{ML}} = \arg \max \mathcal{L}, \quad (4)$$

$$-2 \ln \mathcal{L} = \sum_m \frac{1}{\sigma_m^2} (y_m - f_m(\boldsymbol{\theta}))^2, \quad (5)$$

$$(6)$$

where y_m is the m th component of the observed data \mathbf{y}

$$\mathbf{y} = \mathbf{f}(\boldsymbol{\theta}_{\text{true}}) + \mathbf{n}, \quad (7)$$

under the assumption that $\mathbf{n} = (n_1, \dots, n_M)$ is uncorrelated Gaussian noise

$$\langle n_m \rangle = 0, \quad (8)$$

$$\langle n_m n_{m'} \rangle = \sigma_m^2 \delta_{m,m'}. \quad (9)$$

Asymptotically, maximum likelihood estimators can achieve maximum efficiency. That is, for sufficiently large number of estimates in a set of maximum likelihood estimates $\{\theta_{\text{ML}}\}$, the root-mean-squared error becomes arbitrarily close to the CRLB (see Cramér (1946); Le Cam (1953) for proof).

However, the relation (3) does not necessarily hold for biased estimators. That is, the root-mean-squared-error can be smaller than the CRLB (see Le Cam (1953) for examples). Therefore, we want to investigate the conditions under which, RMSE arising from a given centroiding method becomes close to the CRLB, or whether it can become equal to the CRLB in which case the method is *saturating* the bound, or whether it can drop below the CRLB in which case the method is *beating* the bound.

In this investigation, the observables are the pixel-convolved PSF (PSF profile evaluated at different pixel locations), and the model parameters under consideration are the centroid coordinates. Therefore, \mathcal{F} is a 2×2 matrix whose elements are given by

$$\mathcal{F}_{ij} = \sum_{\mathbf{p}} \frac{1}{\sigma^2} \frac{\partial f_{\mathbf{p}}}{\partial \theta_i} \frac{\partial f_{\mathbf{p}}}{\partial \theta_j}, \quad (10)$$

where the summation is over pixels, $f_{\mathbf{p}}$ is the value of the PSF at pixel location \mathbf{p} , $\theta = \{x_c, y_c\}$, σ^2 is variance of the uncorrelated Gaussian noise map $n(\mathbf{x}_{\mathbf{p}})$

$$\langle n(\mathbf{x}_{\mathbf{p}}) \rangle = 0, \quad (11)$$

$$\langle n(\mathbf{x}_{\mathbf{p}}) n(\mathbf{x}_{\mathbf{p}'}) \rangle = \sigma^2 \delta_{\mathbf{pp}'}. \quad (12)$$

Derivation of an explicit expression for the Fisher matrix \mathcal{F} requires specifying a PSF model. We use the Moffat profile (Trujillo et al. 2001) for our PSF simulations. Moffat profile is an analytic model for stellar PSFs. It has broader wings than a simple Gaussian profile. The surface brightness of the Moffat profile is given by

$$I(r) = \frac{F(\beta - 1)}{\pi \alpha^2} [1 + (r/\alpha)^2]^{-\beta}, \quad (13)$$

where F is the total flux, β is a dimensionless parameter, and α is the length scale of the Moffat profile, with FWHM (hereafter denoted by γ) being $2\alpha\sqrt{2^{1/\beta} - 1}$. At a fixed γ , Moffat profiles with lower values of β have broader tails. It is also important to note that for sufficiently large values of the parameter β , the Moffat PSF becomes arbitrarily close to a simple Gaussian PSF.

In order to investigate the performance of centroiding methods for different background noise levels and different values of the parameter γ , simulation of a large number of images of stars—for which the exact positions of centroids and their corresponding lower bounds are known—is required.

Given the PSF model (13), an expression for the CRLB as a function of the size, and SNR of stars can be derived. For further simplicity, the flux of all stars in our simulations are set to unity and per-pixel uncertainties are assumed to be uncorrelated Gaussian.

Moreover, it is more convenient to work with the signal-to-noise ratio (hereafter denoted by SNR) instead of the variance of the Gaussian noise. We use the definition of SNR according to which, SNR is given by the ratio of the mean and variance of the distribution which the flux estimator is drawn from. Assuming that the total flux from the point source is F , and that the sub-pixel shifted PSF at the i -th pixel is given by P_i . Therefore the brightness of the i -th pixel y_i is drawn from a Gaussian distribution

$$p(y_i) = \mathcal{N}(FP_i, \sigma^2). \quad (14)$$

The optimal estimator of flux is the matched-filter flux estimator $\tilde{F} = \sum_i y_i P_i$. It can be shown that

$$p(\tilde{F}) = \mathcal{N}\left(F, \frac{\sigma^2}{\sum_i P_i^2}\right), \quad (15)$$

which leads us to

$$\text{SNR} = \frac{F\sqrt{\sum_i P_i^2}}{\sigma}. \quad (16)$$

In the case of Moffat profiles (13) with total flux of stars set to unity, SNR given in (16) can be analytically expressed in terms of the per pixel uncertainty σ , FWHM γ , and also β

$$\text{SNR} = \frac{2(\beta - 1)(2^{1/\beta} - 1)^{1/2}}{\pi^{1/2}(2\beta - 1)^{1/2}} \frac{1}{\sigma\gamma}. \quad (17)$$

Equation (17) implies that at a fixed γ and background Gaussian noise with variance σ^2 , stars with broader tails (lower β) have lower SNR. On the other hand, stars with higher value of β have higher SNR. For sufficiently large β —where the PSF can be approximated

by Gaussian profile—SNR is approximately given by $0.664/(\sigma\gamma)$. Furthermore, at a fixed β and variance of the background noise σ^2 , observed stars with higher γ have lower SNR.

Throughout this investigation, β is held fixed at the fiducial value of 2.5, where SNR is given by the following expression

$$\text{SNR} \simeq \frac{0.478}{\sigma\gamma}. \quad (18)$$

Given the analytic expression for the Moffat PSF model (13), and choice of $\beta = 2.5$, the inverse of the Fisher matrix is given by

$$\mathcal{F}^{-1} \simeq \left(0.685 \frac{\gamma}{\text{SNR}}\right)^2 \begin{pmatrix} 1 & 0 \\ 0 & 1 \end{pmatrix}. \quad (19)$$

Equation (19) implies that at given SNR and γ , CRLB for each component of centroid is approximately given by $0.685\gamma/\text{SNR}$, and that a good centroiding technique delivers centroids with root-mean-squared-error (hereafter RMSE) close to this.

It is worth noting that for any PSF model whose radial light profile is some function of r/γ , CRLB has the same functional form, in that it is proportional to the ratio between γ and SNR. For PSF profiles with shorter tails (*e.g.*Gaussian), the prefactor of 0.685 in (19) becomes smaller. In particular case of Gaussian PSF, the prefactor is approximately 0.6.

We examine fitting an exact PSF profile to the stars. That is, in our Cramér-Rao bound saturation tests, we find the best estimates of flux and centroid by optimizing the χ^2 . We expect this method to perform better in determining the centroids of stars, and deliver RMSE very close to Cramér-Rao bound. In the next section, we briefly discuss the centroiding methods used in our Cramér-Rao bound saturating tests.

3. Centroiding methods

Matched filter polynomial centroiding Let us consider the case in which we have a good estimate of the pixel-convolved PSF at the position of the faint star under consideration. We can smooth the image of the star, by correlating it with the full PSF \mathcal{P} at the position of the star.

$$Y^{(s)} = Y \star \mathcal{P}, \quad (20)$$

$$Y_{[i,j]}^{(s)} = \sum_{k,l} Y_{[i-k,j-l]} \mathcal{P}_{[k,l]}, \quad (21)$$

where Y is the image of the star, and $Y^{(s)}$ is called matched filter. Matched filter is a model where the data Y is correlated (convolved in the case of symmetrical PSF) with

the PSF \mathcal{P} . It provides an optimal detection map where the peak of the map is the likely position of the point source (Lang *et al.*, in preparation).

Then, we fit a simple 2d second-order polynomial $P(x, y) = a + bx + cy + dx^2 + exy + fy^2$ to the 3×3 patch centered on the brightest pixel of the matched-filter image Y^s . Upon constructing a universal 9×6 design matrix

$$\mathbf{A} = \begin{bmatrix} 1 & x_1 & y_1 & x_1^2 & x_1y_1 & y_1^2 \\ \cdot & \cdot & \cdot & \cdot & \cdot & \cdot \\ \cdot & \cdot & \cdot & \cdot & \cdot & \cdot \\ \cdot & \cdot & \cdot & \cdot & \cdot & \cdot \\ 1 & x_9 & y_9 & x_9^2 & x_9y_9 & y_9^2 \end{bmatrix}, \quad (22)$$

the free parameters $\{a, b, c, d, e, f\}$ (hereafter compactly denoted by \mathbf{X}) can be determined by

$$\mathbf{X} = (\mathbf{A}^T \mathbf{A})^{-1} \mathbf{A}^T \mathbf{Z}, \quad (23)$$

where \mathbf{Z} is given by $(z_1, \dots, z_9)^T$, with z_i being the brightness of the i -th pixel of the 3×3 patch centered on the brightest pixel of $Y^{(s)}$. Afterwards, the best fit parameters can be used to compute the centroid coordinate

$$\begin{bmatrix} x_c \\ y_c \end{bmatrix} = \begin{bmatrix} 2d & e \\ e & 2f \end{bmatrix}^{-1} \begin{bmatrix} -b \\ -c \end{bmatrix}. \quad (24)$$

It is important to note that the algebraic operation in (24) involves inverting a 2×2 curvature matrix

$$D = \begin{bmatrix} 2d & e \\ e & 2f \end{bmatrix}. \quad (25)$$

When the curvature matrix D has a zero (or very close to zero) determinant, centroid estimates obtained from equation (24) can become arbitrarily large which leads to catastrophic outliers. In order to tackle this issue, we add a soft regularization term proportional to σ^2 to the determinant of D .

The procedure of convolving the image of star with the PSF results in a more well-sampled image, which eventually, leads to having more information regarding the centroids of stars in the 3×3 patch around the brightest pixel. In addition, a simple second-order polynomial will provide a better fit since convolution with the PSF makes the variation of the brightness of the image across the 3×3 patch very smooth.

Default polynomial centroiding In the case that we do not know the PSF at the position of star, we change the smoothing step in the following way. Instead of smoothing

the image by convolving it with the PSF, smoothing is done by convolving the image with a Gaussian kernel of a fixed size

$$k(\mathbf{x}) = \frac{1}{2\pi w^2} \exp(-\mathbf{x}^2/2w^2), \quad (26)$$

where throughout this study, the full-width at half-maximum of the Gaussian kernel is held at a fixed value of 2.8 pixels (corresponding to $w \simeq 1.2$ pixels). Smoothing step is done as follows

$$Y^{(s)} = Y * \mathcal{K}, \quad (27)$$

$$Y_{[i,j]}^{(s)} = \sum_{k,l} Y_{[i-k,j-l]} \mathcal{K}_{[k,l]}, \quad (28)$$

where Y is the image of the star, $Y^{(s)}$ is the smooth image, and \mathcal{K} is a 7×7 array whose elements are given by the Gaussian kernel

$$\mathcal{K}_{[k,l]} = k(x_k, y_l). \quad (29)$$

Then we apply the same 2d second-order polynomial method to the 3×3 patch centered on the brightest pixel of the smooth image $Y^{(s)}$. Therefore, for a given star and a smoothing kernel, the outcome of equation (23) can be plugged into equation (24) to find the centroid estimate of the star. This is inspired by the 3×3 quartic approximation used in the *Sloan Digital Sky Surveys* photometric pipeline (Lupton *et al.* 2001).

Center-of-light centroiding In addition to the methods mentioned so far, we examine centroiding stars by computing their first moments in a 7×7 patch around the brightest pixel of the image.

$$x_c = \frac{\sum_{\mathbf{p}} x_{\mathbf{p}} Y_{\mathbf{p}}}{\sum_{\mathbf{p}} Y_{\mathbf{p}}}, \quad (30)$$

$$y_c = \frac{\sum_{\mathbf{p}} y_{\mathbf{p}} Y_{\mathbf{p}}}{\sum_{\mathbf{p}} Y_{\mathbf{p}}}, \quad (31)$$

where the summation is done over all the pixels of the 7×7 patch, and $x_{\mathbf{p}}$, $y_{\mathbf{p}}$, and $Y_{\mathbf{p}}$, are the x coordinate, y coordinate, and the brightness of pixel \mathbf{p} respectively.

In terms of saturating the Cramér-Rao lower bound, we expect this simple center of light centroiding to perform worse than all other methods mentioned in this section. Hereafter, we call this method 7×7 moment centroiding.

4. Tests

We perform two sets of simulations. In the first set, we choose four values of 2, 2.8, 4, and 5.6 pixels for γ . For each γ , we generate 100,000 17×17 postage-stamps of Moffat profiles with centroids randomly drawn within the central pixel of the 17×17 postage-stamps. Moreover, zero-mean uncorrelated Gaussian noise is added to each postage-stamp such that the simulated stars are uniformly distributed in log-SNR between $\text{SNR} = 5$ to $\text{SNR} = 100$.

In the second set, we generate 100,000 17×17 postage-stamps of Moffat profile, with values of γ uniformly distributed between 2 and 6 pixels, and with centroids drawn randomly within the central pixel. We choose four values for SNR: 5, 10, 20, and 40. For each SNR, and for each postage-stamp with a given γ , zero-mean uncorrelated Gaussian noise, with standard deviation corresponding to SNR and γ through equation (17), is added to each postage-stamp.

In the first experiment, we study how centroiding error behaves with changing SNR, while γ is held constant. In the second experiment, we study how centroiding error behaves with changing γ while SNR is held constant.

5. Results

5.1. Experiment 1

In this experiment, after finding the centroiding error for each method, we compute the RMSE in bins of SNR in order to compare it to the CRLB. Results of the first experiment are shown in Figures [1], [2], [3], [4]. All methods deliver results with RMSE larger for fainter stars.

As we expected, the RMSE from centroiding by fitting the exact PSF model [1] lies on the CRLB except for simulations with $\text{SNR} \lesssim 10$ where the RMSE gets slightly pulled away from the CRLB due to presence of a few outliers. Figure [2] demonstrates that even the matched-filter polynomial centroiding is able deliver centroiding estimates as accurate as PSF profile fitting, with the exception of simulated stars with $\gamma = 2$ pixels. For stars with $\gamma = 2$ pixels, although second-order polynomial fitting gets close to saturating the CRLB, it fails to saturate the CRLB since the PSF is undersampled. For simulated images with higher γ , convolving the data with the PSF result in images that are well-sampled around the brightest pixel. This allows the polynomial centroiding to deliver highly accurate results that can saturate the CRLB for simulated data with $\text{SNR} \gtrsim 10$.

RMSE from the default polynomial centroiding [3], is very close to the CRLB except at the very small values of SNR ($\text{SNR} \lesssim 10$). As we increase γ from 2 pixels to 2.8 pixels, RMSE gets closer to the CRLB. When we increase γ to 4 and 5.6 pixels, RMSE gets farther from the CRLB. For stars with $\gamma = 2$ pixels, the rate at which the RMSE from this method drops eventually becomes smaller than the constant rate at which the CRLB decreases with increasing SNR. The reason for this is that even after smoothing the with a Gaussian kernel, the image is still relatively undersampled, and not smooth enough for a second-order polynomial fitting to provide highly accurate centroiding estimates. For stars with $\gamma = 2.8$ pixels, since the FWHM of the Gaussian kernel matches that of the PSF of underlying simulations, the smooth images are well-sampled and therefore, the method is able to deliver estimates extremely close to saturating the CRLB. As γ gets higher for the simulations, the convolved images are not as well-sampled as those whose γ matches the FWHM of the smoothing kernel and as a result, we loose some information by fitting a second-order polynomial to a 3×3 patch. Therefore, we observe slight deviation from the CRLB for stars with $\gamma = 4$ pixels, and slightly more deviation as we increase γ to 5.6 pixels.

However, in case of 7×7 moment method [4], RMSE becomes quite large as we move towards fainter stars in our simulation. For stars with larger γ , centroid estimates from the naive center of light centroiding show large deviation from saturating the CRLB. By increasing γ , RMSE deviates further away from the CRLB.

5.2. Experiment 2

In this experiment, after finding the centroiding error for each method, we compute the RMSE in bins of γ in order to compare it to the CRLB. Behavior of error as a function of γ for different values of SNR, is shown in figures [5], [6], [7], and [8].

Once again, the RMSE from centroiding by fitting the exact PSF model as a function of FWHM perfectly lies on the CRLB except at $\text{SNR} = 5$ where the RMSE slightly deviates from the CRLB due to presence of a few outliers [5]. Thus, centroid estimates from fitting the exact PSF model always saturate the CRLB. Once again, we observe that the centroid estimates found by matched-filter polynomial centroiding saturate the CRLB with the exception of simulated stars with $\text{SNR} = 5$, or γ very close to 2 pixels [6].

The default polynomial method [7], results in RMSE very close to the CRLB. For all four values of SNR, as we increase γ from 2 pixels to 3 pixels, RMSE gets slightly closer to the CRLB since the method starts to perform slightly better as we move away from undersampled stars, and as the FWHM of the smoothing kernel gets closer to that of the

simulated images. After approximately 3 pixels, increasing γ results in deviation of RMSE of the method from the CRLB. This is a characteristic of polynomial method as we apply it to a smooth image which is still not sufficiently well-sampled. Furthermore, increasing SNR from 5 to 40 makes the RMSE (as a function of γ) become closer to the CRLB. In the case of extremely faint stars (SNR = 5), default polynomial centroiding is not able to deliver any reliable estimate, and it fails.

The centroid estimates obtained from the naive 7×7 moment method [8] result in RMSE much larger than the CRLB in all ranges of FWHM and for all four values of SNR in this experiment.

6. Discussion

An optimal stellar centroiding algorithm must saturate the fundamental Cramér-Rao lower bound. That is, in all ranges of background noise level, size, radial light profile, and shape, it must preserve information about the centroids of stars. In practice however, this is only achievable when we have a reasonably good estimate of the PSF. Since, we do not always know the exact PSF profile, we make use of various approximate centroiding algorithms. In this work, we studied how different methods come close to saturating the CRLB for relatively low signal-to-noise ratio unsaturated stars.

We focused on examples from two classes of centroiding algorithms. The first class contains fast and approximate methods that do not require any knowledge of the PSF at the positions of stars. Of methods that belong to this class, we consider centroiding stars based on fitting a second-order polynomial to a 3×3 patch of star images smoothed by a Gaussian kernel of fixed width, and finding the center of light of a 7×7 patch around the brightest pixel of the star. The second class of centroiding algorithms contains methods that require knowledge of the PSF (or having a good estimate of the PSF) at the positions of stars. We considered two examples from this class. The first example is the matched-filter polynomial centroiding, and the second example is the full PSF profile fitting. In terms of saturating the Cramér-Rao bound, we compared the performances of these methods against each other.

Our results suggest that in all ranges of FWHM and SNR, the PSF fitting method returns centroid estimates that saturate the CRLB; with the exception of SNR being less than 10, in which case a few centroiding outliers caused the RMSE to slightly, but not significantly, deviate from the CRLB. We found that the estimates found by 7×7 moment method, except in the case of very high SNR values and very small ranges of γ , do not come close to saturating the CRLB. In a considerable range of PSF sizes and background noise

levels, this method fails to deliver any reliable centroiding estimates.

On the other hand, the RMSE of centroid estimates of default polynomial centroiding are much closer to saturating the CRLB in all ranges of signal-to-noise ratio. The performance of this method however, is limited by two important factors: *(i)* signal-to-noise ratio, and *(ii)* PSF size. The default polynomial centroiding technique only takes advantage of the information contained in a 3×3 patch centered on the brightest pixel of the smoothed image which is only well-sampled when the FWHM of the simulated image of star matches that of the smoothing kernel. Thus, when we apply this method to find the centroids of stars with larger FWHM, certain amount of information (encoded in the Cramér-Rao lower bound) is lost, and therefore, the RMSE of these methods deviates from the CRLB. This deviation becomes even larger at lower signal-to-noise ratios. Besides, the performance of this method slightly degrades in the case of undersampled stars (with FWHM close to 2 pixels). Presence of noise is another limiting factor. Although this method is able to get very close to saturating the CRLB in a wide range of signal-to-noise ratios, it is not reliable in the case of centroiding extremely faint stars. This is partly due to the fact that in the presence of noise, the brightest pixel of image does not necessarily contain the centroid of stars even after smoothing the image.

Once we modify the polynomial method further by convolving the image with the full postage stamp of the PSF, we obtain results that saturate the CRLB in a wide range of PSF sizes and noise levels. This is due to the fact that once the images of stars are convolved with the correct PSF, they become so well-sampled and smooth that fitting a second-order polynomial to the 3×3 patch centered on the brightest pixel of the smooth image is sufficient for us to obtain results as accurate as those from fitting a PSF profile. The only conditions in which slight deviation from saturating the CRLB occurs are very low signal-to-noise ratios ($\text{SNR} \lesssim 10$), and undersampled PSF ($\text{FWHM} \sim 2$ pixels). One advantage of this method over PSF fitting method is that it is fast, and that it is able to saturate the CRLB in a wide range of conditions. In the case that we have a good estimate of the PSF, the matched-filter polynomial centroiding is a significantly much faster algorithm. Although this method is more accurate than default polynomial centroiding, it is slightly slower because it requires convolution of the image with the full postage stamp of the PSF.

In this investigation we showed that PSF fitting always performs better—in terms of saturating the CRLB—at centroiding stars. However, this method has its own disadvantages. First, we do not always know the exact PSF. Second, finding the centroid by profile fitting is computationally expensive, whereas employing any of the 3×3 polynomial techniques considered in this study in large scale astronomical surveys reduces the computational cost of initial astrometry of the point sources considerably.

Moreover, it is important to note that the PSF fitting method can be made faster by only keeping the term proportional to the dot product of the PSF model and the image in χ^2 . This is because the other terms in χ^2 are not sensitive to the position of the centroid. However, this only allows us to vary the position of centroid, and not the flux, while fitting the PSF model to the star.

Modifying the χ^2 such that it contains the dot product of the PSF and image, provides a nice interpretation for the PSF fitting method. It corresponds to searching for the centroid in a very high resolution grid which the dot product of the image and the PSF model is sensitive to. On the other hand, one can think of the initial smoothing step in the default polynomial method as upsampling of the image around the center by convolving it with an approximate Gaussian PSF. The default polynomial centroiding is different from PSF-fitting method in that, when there is mismatch between the widths of the smoothing kernel and the that of the PSF, we loose some information by employing a 3×3 polynomial fitting. When we have the advantage of knowing the PSF, this issue can be resolved by employing the matched-filter polynomial method.

Having a reasonable PSF model always helps us obtain more reliable centroid estimates, but over a certain range of low signal-to-noise ratios and PSF sizes, one can achieve sensibly accurate results by employing a simple 3×3 method after smooting the image with a Gaussian kernel of a fixed width, and without making any assumption about the PSF model at the positions of stars.

In this investigation we narrowed our focus on a set of data simulated from a particular PSF profile. Although there are various cases where Moffat profiles provide reasonable representations of the point spread function, these profiles are not generic enough to let us reach a more general conclusion. Another important, and untapped, area of study would be devising a model that infers the centroids of stars and point spread function—in its full extent, not at the catalog level—across an astronomical image simultaneously. This is beyond the scope of this study.

This work was partially supported by the NSF (grants IIS-1124794 and AST-1517237), NASA (grant NNX12AI50G), and the Moore-Sloan Data Science Environment at NYU. We thank Jo Bovy for useful discussions.

REFERENCES

Bertin, E., Arnouts, S. 1996 *Astronomy and Astrophysics Supplement Series*, 117, 393-40

Cramér, H. 1946 *Mathematical methods of statistics*, Princeton university press

Le Cam, L. M. 1953 On some asymptotic properties of maximum likelihood estimates and related Bayes' estimates (Vol. 1, No. 11), University of California press

Lupton, R. et al. 2001 arXiv: astro-ph/0101420

Schechter, P. L., Mateo, M., Saha, A. 1993 PASP, 1342-1353

Stetson, P. B. 1987, PASP, 191-222

Trujillo, I., et al. 2001 MNRAS, 977-985

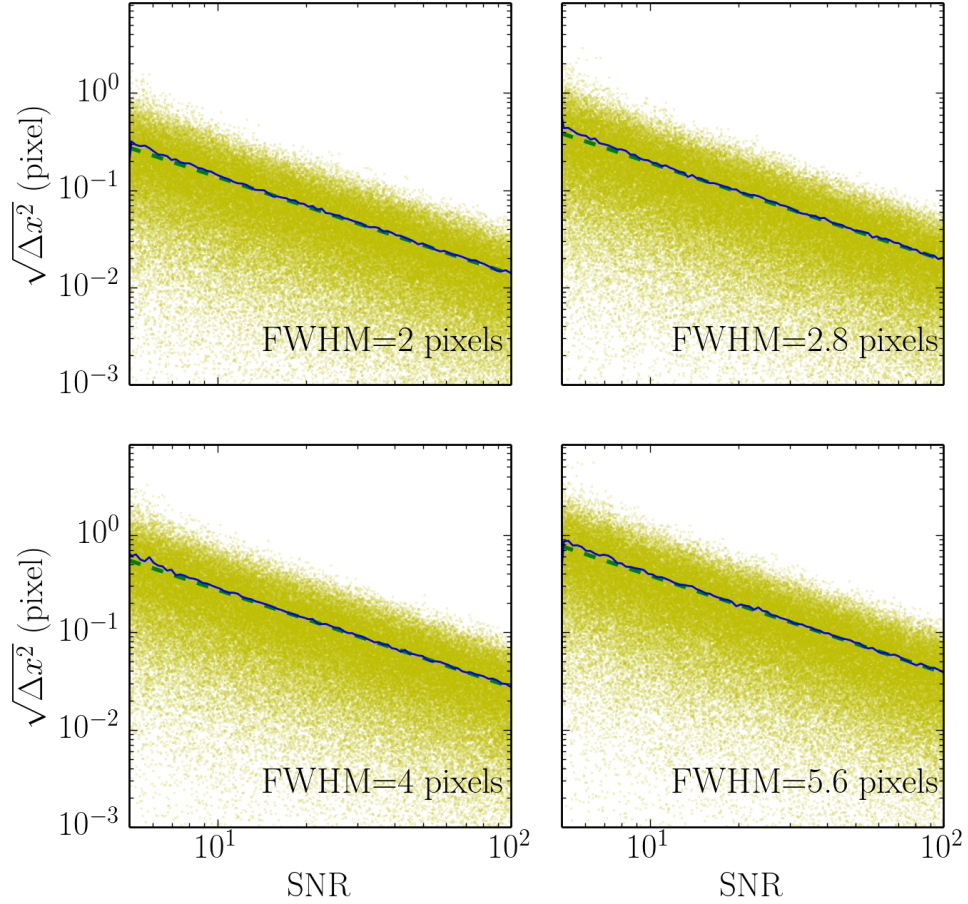


Fig. 1.— Scatter plots showing the relation between error in centroid measurement from fitting the exact PSF model to the stars and the signal-to-noise ratio of stars, with FWHM of : 2 (upper left), 2.8 (upper right), 4 (lower left), and 5.6 (lower right) pixels. In each scatter plot, the blue solid line represents the root-mean-squared-error, and the green dashed line represents CRLB.

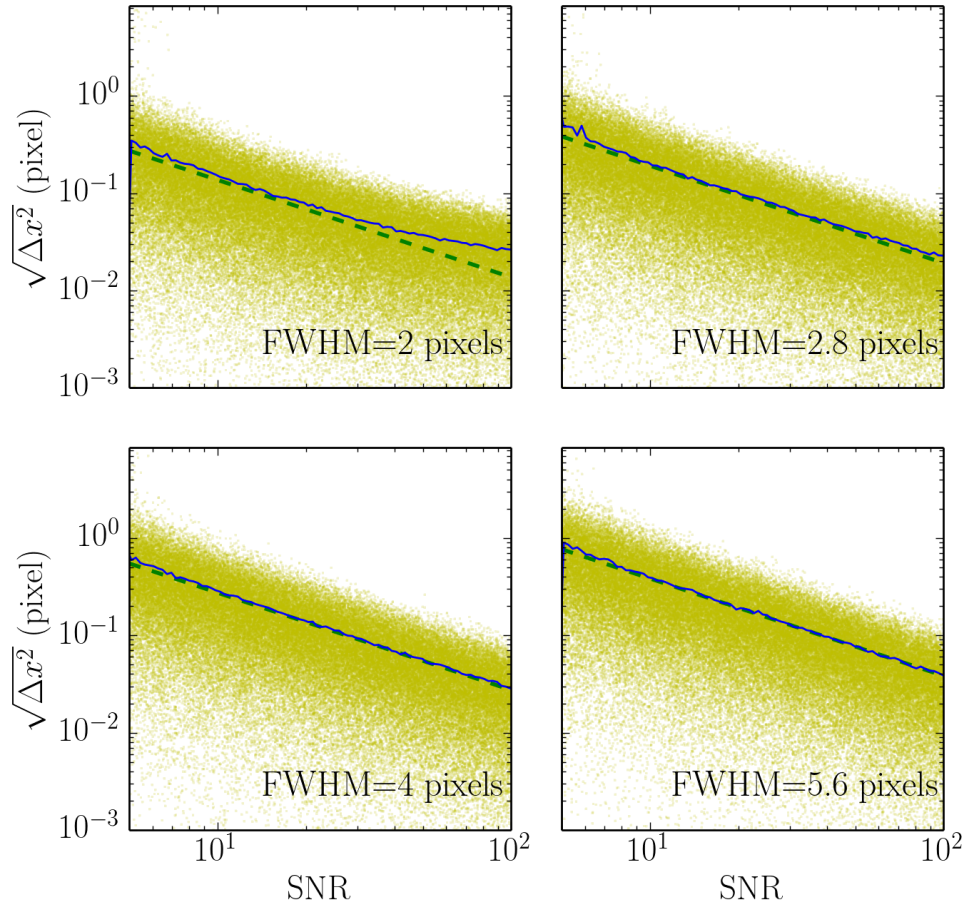


Fig. 2.— Scatter plots showing the relation between error in centroid measurement from the PSF-based 3×3 polynomial method and the signal-to-noise ratio of stars, with FWHM of : 2 (upper left), 2.8 (upper right), 4 (lower left), and 5.6 (lower right) pixels. In each scatter plot, the blue solid line represents the root-mean-squared-error, and the green dashed line represents CRLB.

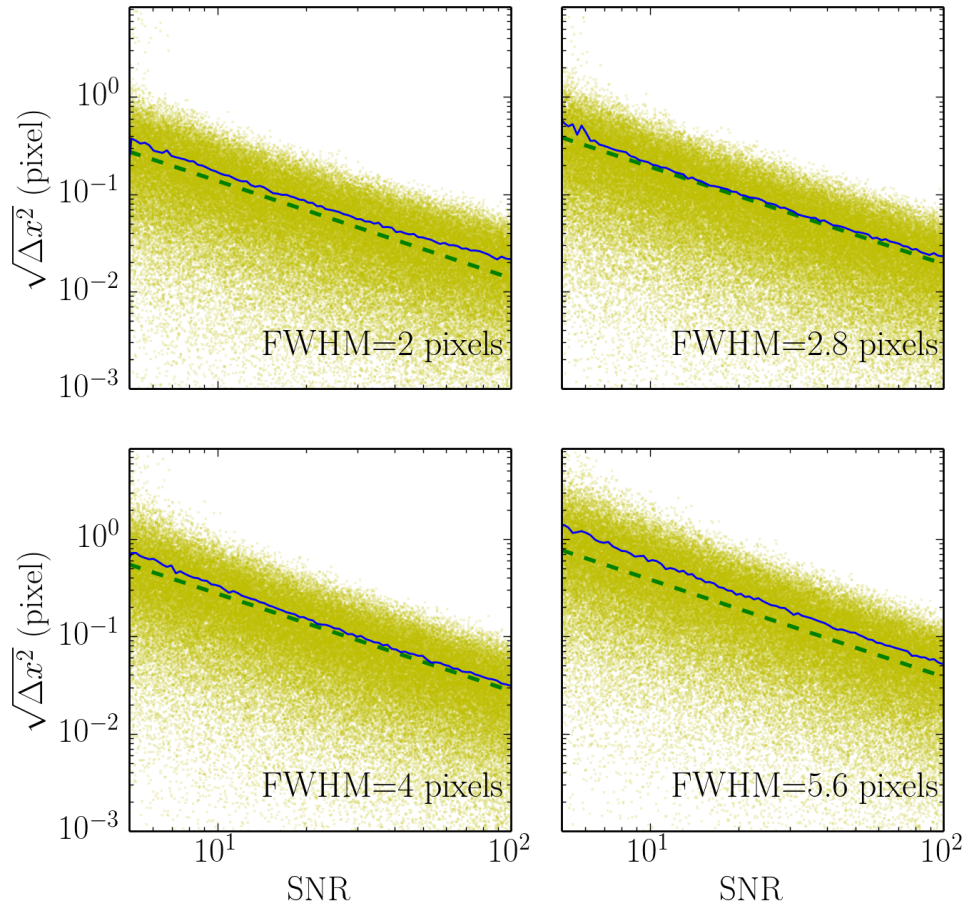


Fig. 3.— Scatter plots showing the relation between error in centroid measurement from the 3×3 polynomial centroiding and the signal-to-noise ratio of stars, with FWHM of : 2 (upper left), 2.8 (upper right), 4 (lower left), and 5.6 (lower right) pixels. In each scatter plot, the blue solid line represents the root-mean-squared-error, and the green dashed line represents CRLB.

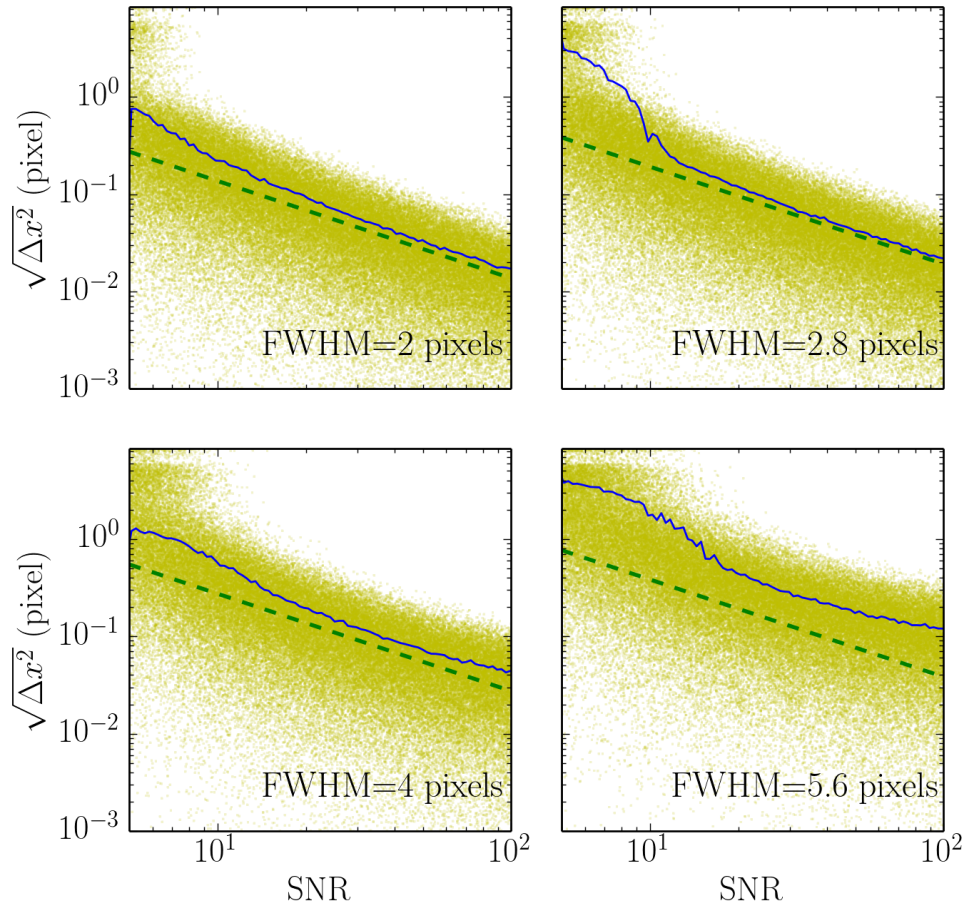


Fig. 4.— Scatter plots showing the relation between error in centroid measurement from the 7×7 moment method and the signal-to-noise ratio of stars, with FWHM of : 2 (upper left), 2.8 (upper right), 4 (lower left), and 5.6 (lower right) pixels. In each scatter plot, the blue solid line represents the root-mean-squared-error, and the green dashed line represents CRLB.

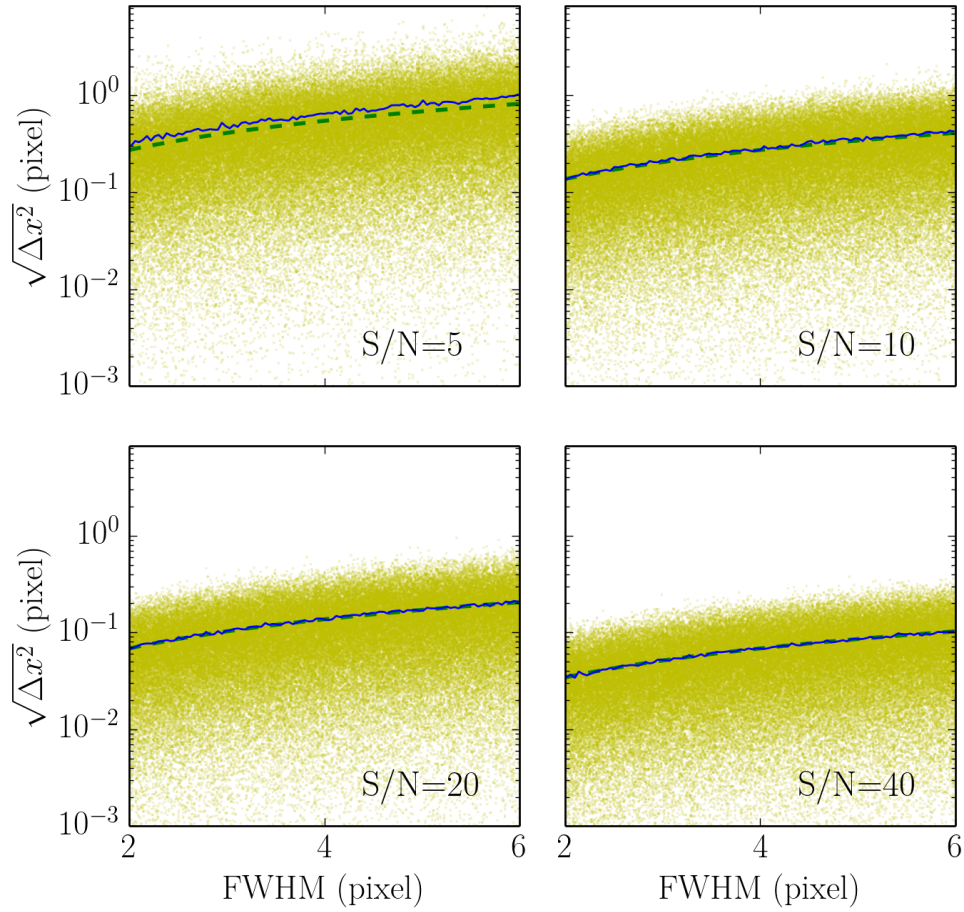


Fig. 5.— Scatter plots showing the relation between error in centroid measurement from fitting the exact PSF model and FWHM of stars, with SNR of : 5 (upper left), 10 (upper right), 20 (lower left), and 40 (lower right). In each scatter plot, the blue solid line represents the root-mean-squared-error, and the green dashed line represents CRLB.

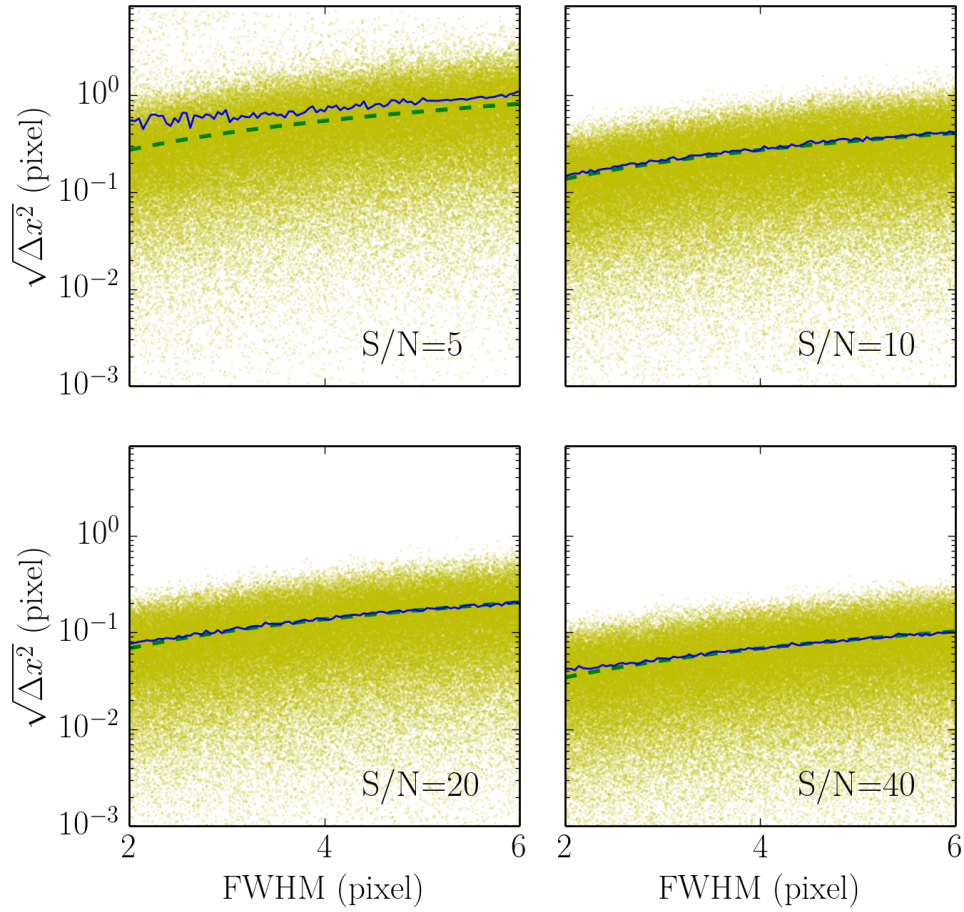


Fig. 6.— Scatter plots showing the relation between error in centroid measurement from the PSF-based 3×3 polynomial method and FWHM of stars, with SNR of : 5 (upper left), 10 (upper right), 20 (lower left), and 40 (lower right). In each scatter plot, the blue solid line represents the root-mean-squared-error, and the green dashed line represents CRLB.

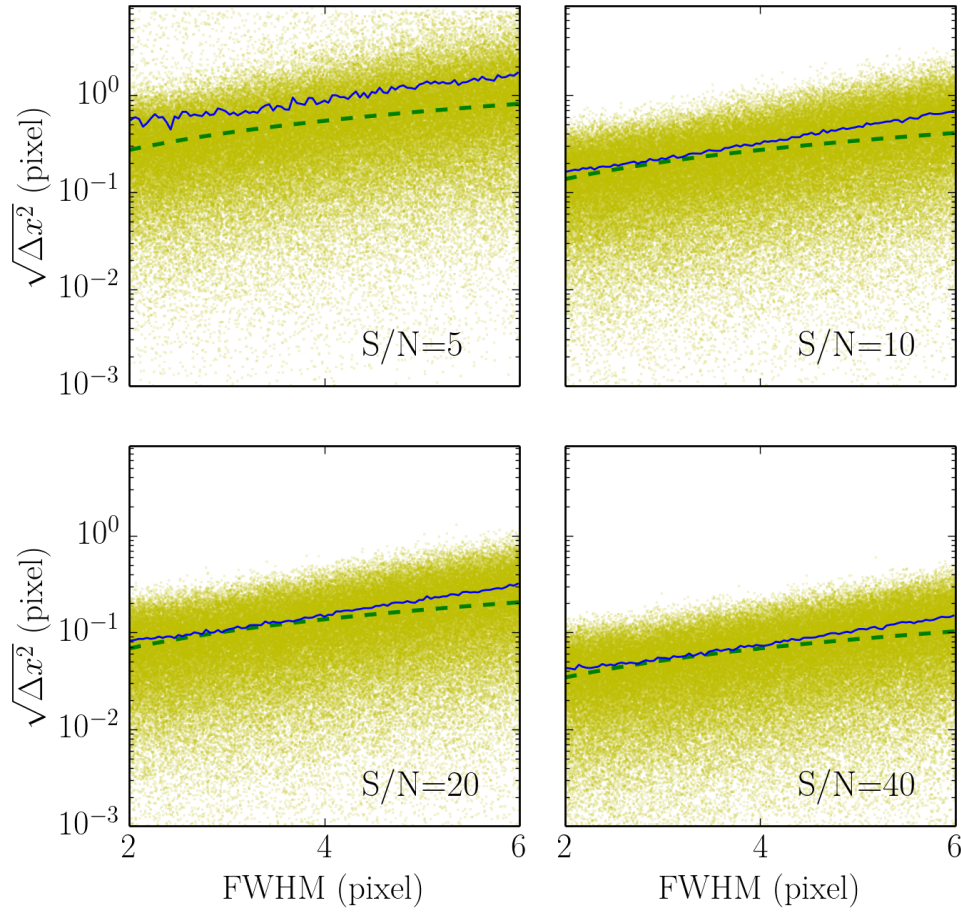


Fig. 7.— Scatter plots showing the relation between error in centroid measurement from the 3×3 polynomial centroiding and FWHM of stars, with SNR of : 5 (upper left), 10 (upper right), 20 (lower left), and 40 (lower right). In each scatter plot, the blue solid line represents the root-mean-squared-error, and the green dashed line represents CRLB.

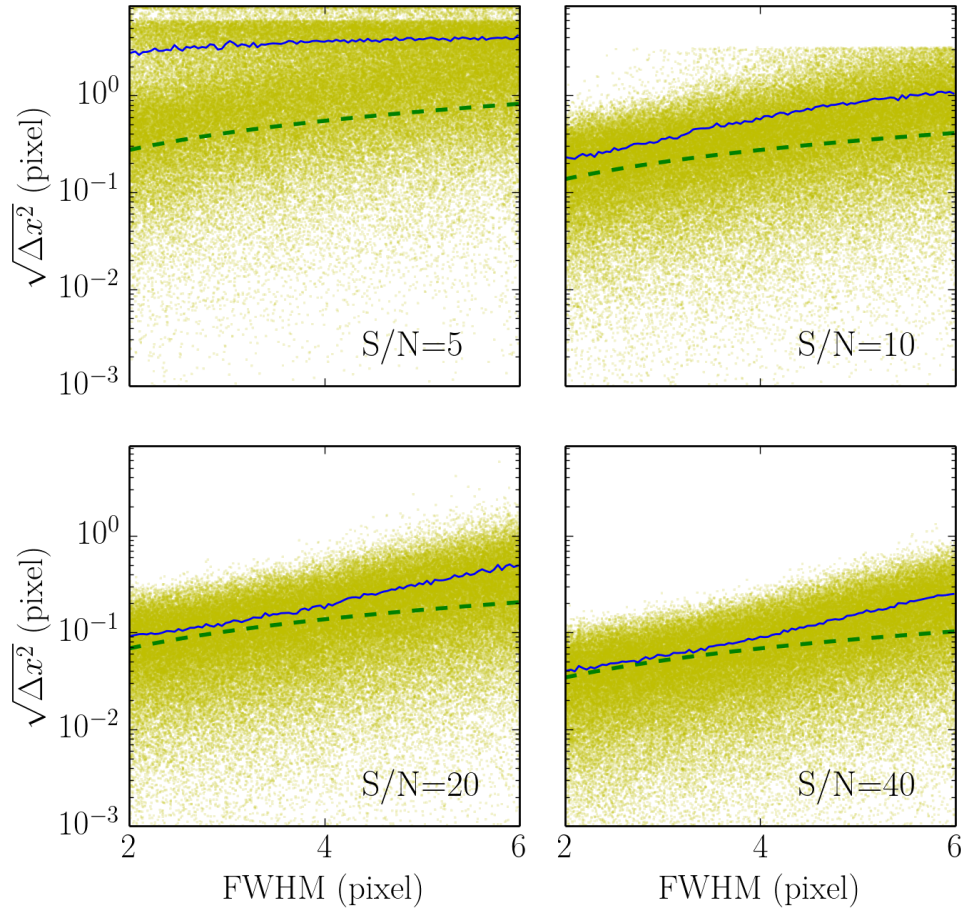


Fig. 8.— Scatter plots showing the relation between error in centroid measurement from the 7×7 moment method and FWHM of stars, with SNR of : 5 (upper left), 10 (upper right), 20 (lower left), and 40 (lower right). In each scatter plot, the blue solid line represents the root-mean-squared-error, and the green dashed line represents CRLB.